



Open Archive Toulouse Archive Ouverte

OATAO is an open access repository that collects the work of Toulouse researchers and makes it freely available over the web where possible

This is an author's version published in: <http://oatao.univ-toulouse.fr/20656>

Official URL:

<https://doi.org/10.1063/1.870295>

To cite this version:

Jounet, Arnaud and Mojtabi, Abdelkader and Ouazzani, Jalil and Zappoli, Bernard Low-frequency vibrations in a near-critical fluid. (2000) *Physics of Fluids*, 12 (1). 197-204. ISSN 1070-6631

Any correspondence concerning this service should be sent to the repository administrator: tech-oatao@listes-diff.inp-toulouse.fr

Low-frequency vibrations in a near-critical fluid

Arnaud Jounet^{a)} and Abdelkader Mojtabi

Institut de Mécanique des Fluides de Toulouse, UMR 5502 CNRS/INP-UPS, UFR MIG, Université Paul Sabatier, 118 Route de Narbonne, 31062 Toulouse Cedex, France

Jalil Ouazzani

Arcofluid, Les Bureaux de l'Arche, 5 Rue des allumettes, 13086 Aix-en-Provence Cedex 02, France

Bernard Zappoli

Institut de Mécanique des Fluides de Toulouse, UMR 5502 CNRS/INP-UPS, UFR MIG, Université Paul Sabatier, 118 Route de Narbonne, 31062 Toulouse Cedex, France and Centre National d'Etudes Spatiales, 18 Avenue Edouard Belin, 31405 Toulouse Cedex 04, France

The response of a near-critical fluid to low-frequency vibrations is investigated by means of numerical simulations. Its characteristics are first established by one-dimensional analysis. It is shown that the strong thermo-mechanical coupling occurring in the boundary layers tends to make the fluid oscillate homogeneously at low frequencies, and with a larger amplitude than in a normal gas. The numerical results obtained in this first part are found to confirm earlier predictions made in pioneering theoretical work. Then, the study is extended to a two-dimensional configuration. In a square cavity, the wall shear stresses developing along the longitudinal boundaries do not affect the one-dimensional regime, since the viscous layer present in these areas behaves like the Stokes boundary layer. By contrast, thermostating these boundaries, like the others, generates local curvature of the stream lines. The fluid response to the homogeneous acceleration field then takes some more pronounced two-dimensional patterns, but remains driven by the strong alternating expansions and retractions of the fluid in the thermal boundary layers, which are specific to near-critical fluids. © 2000 American Institute of Physics. [S1070-6631(00)00901-6]

I. INTRODUCTION

For a decade, investigations concerning critical phenomena have shown that heat and mass transfer in a pure fluid near its liquid–vapor critical point is very specific. In particular, experiments performed in microgravity^{1–4} have led to the conclusion that the temperature of a near-critical fluid submitted to heating or cooling from the outside of its container responds quickly despite its very low thermal diffusivity. This phenomenon has been theoretically discussed, using thermodynamical considerations⁵ or from the asymptotic analysis of the Navier–Stokes equations.⁶ It is based on the anomalies of transport properties near the critical point. The thermal diffusivity of near-critical fluids becomes very small on approaching the critical point, but their compressibility and their thermal-expansion coefficients diverge at the same time. As a consequence, when heat is injected into a near-critical fluid, the fluid located in the thin thermal boundary layer strongly expands, compressing the rest of the fluid (the bulk) adiabatically. The compression wave involves a rapid and homogeneous rise of the temperature, which is significant on a much shorter time scale than diffusion. This mechanism has been called the “piston effect,” and since effects linked to compressibility become increasingly intense compared to those of diffusion when approaching the critical

point, it is responsible for the observed critical speeding up of the thermal relaxation instead of the expected critical slowing down. On the other hand, it has been shown that when a near-critical fluid is submitted to heating in a noninsulated cell, the piston effect is responsible for a strong critical speeding-up of heat transfer which can make the fluid behave ultimately like a thermal short-circuit.⁶

In the presence of gravity, two-dimensional numerical studies^{7,8} have shown that the thermoacoustics are still efficient. Thermoconvective instabilities do not prevent the piston effect from heating the fluid, while convective heat transfer remains very poor close to the critical point, and only contributes to mass equilibration. This research has also stressed the complexity of near-critical fluid hydrodynamics, as first discussed twenty years ago.⁹ Recently, the numerical study of the Rayleigh–Bénard configuration¹⁰ has shown that, besides the high compressibility of the fluid, the piston effect can itself contribute to triggering the instability.

Our purpose here is to extend our understanding of near-critical fluid dynamics. Until now, almost all studies related to heat and mass transfer in near-critical fluids have been performed in a configuration in which the fluid state is disturbed by a temperature inhomogeneity. The response of the fluid to a purely mechanical disturbance was only first studied a few years ago by Carlès and Zappoli.¹¹ Those authors considered a one-dimensional near-critical fluid layer submitted to vibrations in a thermostatted cell. Again, their analysis pointed out a peculiar regime, which cannot be wit-

^{a)} Author to whom correspondence should be addressed. Phone: 05.61.55.82.33; fax: 05.61.55.83.26; electronic mail: jounet@lm2f.ups-tlse.fr

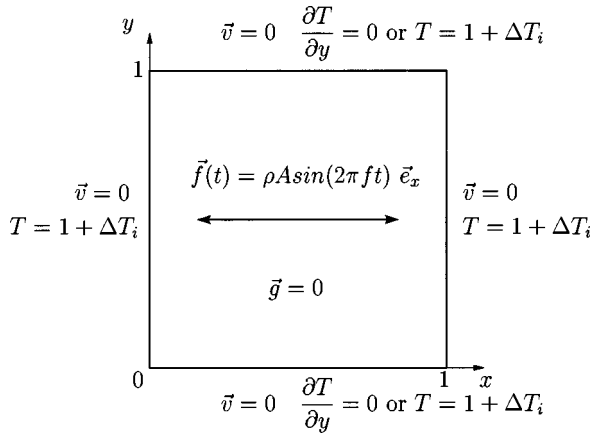


FIG. 1. Configuration.

nessed in normally compressible fluids. They showed that, due to the strong thermomechanical coupling occurring in the boundary layers at low frequencies, the fluid tended to oscillate like a solid body between the two boundary layers, the behavior of which could be compared to that of dampers.

In the present paper, we aim to show the influence of the presence of walls parallel to the acceleration field on the regime described above. By means of numerical simulations, we study the response of the fluid to low-frequency vibrations in a square cavity for two kinds of thermal boundary conditions along the longitudinal walls.

In Sec. II, we first present the general model used for our investigations. The results obtained in a one-dimensional slab-shaped container are recalled in Sec. III, with a special emphasis on the low-frequency specific regime. In Sec. IV, this low-frequency regime is studied in the two-dimensional case. We report the new model utilized for this purpose, and then show our results when the supplementary boundaries are either adiabatic or thermostatted. In Sec. V we summarize the findings obtained in the present paper and conclude.

II. MODEL

The model used in the present analysis is that already presented in previous publications.^{6–8,11}

The van der Waals equation of state is used to take into account the anomalous behavior of many equilibrium parameters close to the critical point, especially the divergence of

the isothermal compressibility K_T , that of the dilation coefficient β and that of the specific heat at constant pressure C_p .

Then, the nondimensional unsteady conservation equations for a viscous heat-conducting compressible fluid can be written on the acoustic time scale as

$$\frac{\partial \rho}{\partial t} + \nabla \cdot (\rho \vec{v}) = 0, \quad (1)$$

$$\frac{\partial(\rho \vec{v})}{\partial t} + \nabla \cdot (\rho \vec{v} \otimes \vec{v}) = -\gamma_0^{-1} \nabla P + \epsilon \left[\nabla^2 \vec{v} + \frac{1}{3} \nabla(\nabla \cdot \vec{v}) \right] + \vec{f}, \quad (2)$$

$$\begin{aligned} \frac{\partial(\rho T)}{\partial t} + \nabla \cdot (\rho \vec{v} T) = & -(\gamma_0 - 1) \left(P + \frac{9}{8} \rho^2 \right) (\nabla \cdot \vec{v}) \\ & + \frac{\epsilon \gamma_0}{\text{Pr}_0} \nabla \cdot [\lambda \nabla T] + \epsilon \gamma_0 (\gamma_0 - 1) \Phi, \end{aligned} \quad (3)$$

$$P = \frac{\rho T}{1 - \rho/3} - \frac{9}{8} \rho^2, \quad (4)$$

in which \vec{f} represents the imposed force field and Φ the dissipation function.

This system is obtained with the following nondimensionalization (concerning density, temperature, pressure and velocity):

$$\rho = \frac{\rho'}{\rho'_c}, \quad T = \frac{T'}{T'_c}, \quad P = \frac{P'}{\rho'_c R' T'_c}, \quad \vec{v} = \frac{\vec{v}'}{c'_0},$$

and the independent variables space and time:

$$\vec{x} = \frac{\vec{x}'}{L'}, \quad t = \frac{t'}{t'_a},$$

the prime (') denoting dimensional parameters [ρ'_c , T'_c and P'_c are the critical coordinates, R' the perfect gas constant divided by the molar mass of the substance, $c'_0 = (\gamma_0 R' T'_c)^{1/2}$ the reference sound velocity (γ_0 is the ratio of the specific heats in the absence of divergence), L' the characteristic length and $t'_a = L'/c'_0$ a typical acoustic time].

The nondimensional parameters present in Eqs. (2) and (3) are defined as

$$\text{Pr}_0 = \frac{\mu'_0 C'_{p0}}{\lambda'_0}, \quad \epsilon = \frac{t'_a}{t'_d} \text{Pr}_0,$$

with

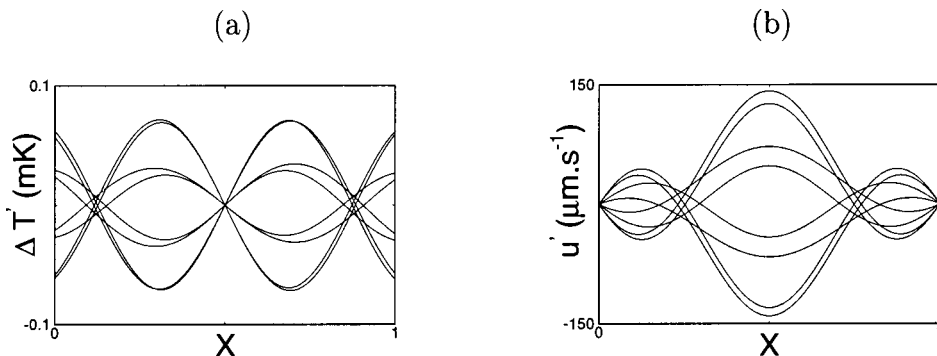


FIG. 2. Temperature and velocity profiles every 1/8th of a period for high-frequency vibrations ($f' = 30$ kHz, $\Delta T'_i = 0.1$ K, $A' = 10$ m s⁻²).

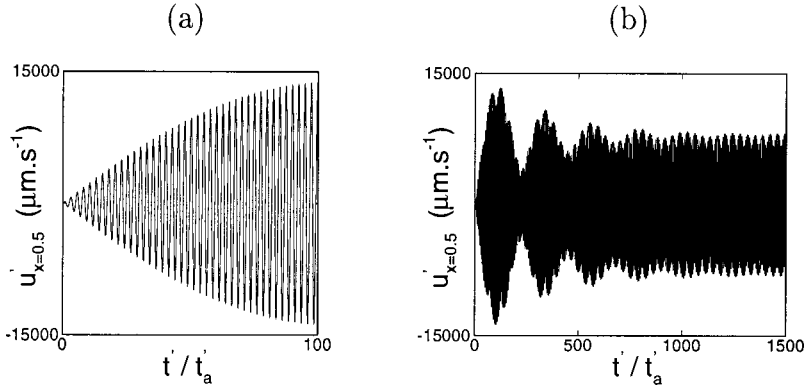


FIG. 3. Velocity variations for a resonant frequency (acoustic regime): (a) resonance and (b) saturation ($f' = 11500$ Hz, $\Delta T'_i = 0.1$ K, $A' = 10$ m s $^{-2}$).

$$t'_d = L'^2 \frac{\rho'_c C'_{P_0}}{\lambda'_0}.$$

Pr_0 is a reference Prandtl number (μ'_0 , C'_{P_0} , λ'_0 are the dynamic viscosity, the specific heat at constant pressure and the thermal conductivity, respectively, in the absence of critical anomalies) and ϵ a small parameter in which t'_d represents a reference diffusion time.

λ is the nondimensional thermal conductivity. Its critical divergence is introduced by

$$\lambda = \frac{\lambda'}{\lambda'_0} = 1 + 0.75 \left(\frac{T' - T'_c}{T'_c} \right)^{-1/2}.$$

The critical exponent of 1/2 differs from that of a real substance (0.64), as do those deduced from the van der Waals equation of state for other properties. But, as explained elsewhere,^{6,7,11} our purpose is to possess a relatively simple model to describe the main features of near-critical singular dynamics, such as strong thermomechanical coupling. Thus, the low divergence of the coefficients of viscosity or that of the specific heat at constant volume are also ignored.

For the problem under consideration, the fluid is initially at rest near the critical point. The initial conditions are

$$T(t=0) = 1 + \Delta T'_i,$$

$$\rho(t=0) = 1,$$

$$P(t=0) = \frac{3}{2}(1 + \Delta T'_i) - \frac{9}{8},$$

$$\vec{v}(t=0) = 0$$

(5)

[$\Delta T'_i = (T'_i - T'_c)/T'_c$, with T'_i the initial temperature].

Since we are interested in the response of the fluid in the absence of gravity, the only source term is imposed through a sinusoidal acceleration (see Fig. 1), that implies

$$\vec{f} = \rho A \sin(2\pi f t) \vec{e}_x, \quad (6)$$

with

$$A = \frac{A' L'}{\gamma_0 R' T'_c} \quad \text{and} \quad f = f' t'_a,$$

the nondimensional amplitude and frequency of the acceleration field.

The walls in the direction perpendicular to the vibration are thermostatted, so that

$$T(x=0) = T(x=1) = 1 + \Delta T'_i. \quad (7)$$

The walls parallel to the vibration are either adiabatic or thermostatted (see Sec. IV), while the nonslip condition at the walls can be written as

$$\vec{v}(x=0) = \vec{v}(x=1) = \vec{v}(y=0) = \vec{v}(y=1) = 0. \quad (8)$$

Calculations have been performed for CO $_2$ ($T'_c = 304.13$ K, $\rho'_c = 467.8$ kg m $^{-3}$, $R' = 188.8$ J kg $^{-1}$ K $^{-1}$) with $L' = 10$ mm. Then, $\epsilon = 2.59 \cdot 10^{-8}$ and $Pr_0 = 2.274$ in the whole study.

III. ONE-DIMENSIONAL RESULTS

To clarify the problem under study, we first briefly present the different regimes appearing as a function of the frequency when the presence of the longitudinal boundaries

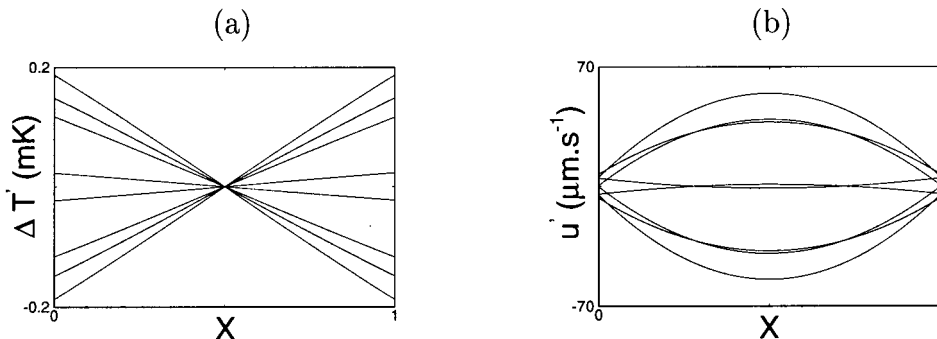


FIG. 4. Temperature and velocity profiles in the bulk fluid for the medium regime ($f' = 3$ kHz, $\Delta T'_i = 0.1$ K, $A' = 10$ m s $^{-2}$).

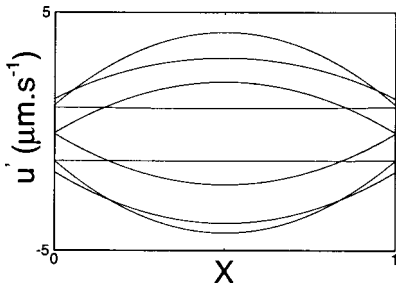


FIG. 5. Velocity in the bulk fluid when the frequency is decreased ($f' = 200$ Hz, $\Delta T'_i = 0.1$ K, $A' = 10$ m s $^{-2}$).

is not taken into account (one-dimensional fluid layer; here, in the x -direction). The configuration is thus the same as that considered in Ref. 11, which reported analytically obtained pioneering results that we therefore aim to confirm here.

Calculations are performed using a finite-volume¹² numerical code, with the SIMPLE algorithm¹³ applied with the stabilization procedure of the Thomas algorithm¹⁴ described in Ref. 15, and with a small mesh around the thermostatted boundaries ($x=0$ and $x=1$) because of the very low diffusivity of near-critical fluids.

A. The acoustic regime

At high frequencies (typically, a few tens of kHz), the vibration characteristic time becomes of the same amplitude or smaller than the acoustic time. Then, as shown in Fig. 2, compression and expansion waves propagate back and forth in the fluid due to the very rapid motion of the cell. As discussed in Ref. 11, the temperature fluctuations are too fast in this regime for the thermal boundary layer to have time to form. Thus, the walls $x=0$ and $x=1$ are adiabatic, and the fluid response would have been the same in a perfect gas. Figure 3 also illustrates that resonance can occur for specific frequencies, as previously shown analytically.¹¹ The numerical simulation here highlights the saturation of this resonance.

B. The medium regime

When decreasing the frequency, a regime of periodic linear oscillations around a vibration node centered in the middle of the cell appears for pressure, density and temperature [Fig. 4(a)]. The pressure gradient oscillation in the bulk generates an almost parabolic oscillating velocity profile [Fig. 4(b)], the amplitude of which decreases with the frequency (Fig. 5). Nevertheless, it can be noted that the velocity at the edge of the thermal boundary layers, which are too thin to appear in Fig. 4(a), is not zero and becomes higher compared to the velocity at the cell center as the frequency decreases. This nonzero velocity is linked to the specific thermomechanical coupling occurring from the boundary layers in near-critical fluids, which becomes prominent at low frequency, as discussed below.

C. The quasi-solid regime

At lower frequencies or closer to the critical point, bulk fluid oscillations tend to become homogeneous (Fig. 6). The

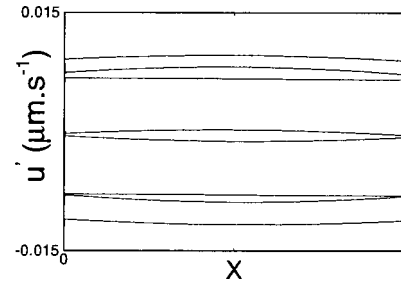


FIG. 6. Velocity profiles in the bulk fluid for the quasi-solid regime, over one period of oscillation every 1/8th of a period ($f' = 5$ Hz, $\Delta T'_i = 15$ mK, $A' = 0.1$ m s $^{-2}$).

flat velocity profiles are driven by the thermal boundary layers. Some oscillating boundary layers form due to the linear temperature oscillations in the bulk fluid. The temperature oscillations in the boundary layers provoke strong oscillations of density illustrating fluid dilation [Figs. 7(a) and 7(b)]. In turn, thermal expansion (or contraction) is responsible for the presence of oscillating dynamic boundary layers [Fig. 7(c)], the velocity at the edge of which becomes much larger than that caused by the linear pressure gradient in the bulk. This regime appears in near-critical fluids when the vibration characteristic time is equal to or smaller than the piston effect time,^{11,6} that is to say, when the thermomechanical coupling specific to near-critical fluids has time to develop.

D. Summary

The three different responses demonstrated above can be summarized in Fig. 8, which represents the maximum velocity as a function of the frequency.

One characteristic of the high-frequency regime is that u'_{\max} decreases as the frequency increases, except for special values of the frequency at which resonance occurs.

At lower frequencies, two regimes can be distinguished. Asymptotically, the first exhibits a linear dependence of u'_{\max} on f' : this is the medium regime, in which the results obtained are close to those appearing in a perfect gas¹⁶ (parabolic velocity profiles). Nevertheless, the density gradients generated in the boundary layers are very large due to the strong dilation occurring in near-critical fluids, that which might, in addition, speed up the corrosion of the container walls.¹⁷

Finally, when decreasing the frequency, u'_{\max} tends to decrease like the square root of f' . This nonlinear regime is completely specific to near-critical fluids since it is associated to the strong thermal expansion or contraction of the fluid in the boundary layers. The dynamic response of the fluid to the acceleration field then no longer originates in the bulk. Since, when one boundary layer expands, the opposite one contracts, the bulk is simultaneously pushed on one side and pulled on the other. Hence, it tends to oscillate at a uniform velocity, like a block of solid matter between two highly compressible boundary layers. This regime appears clearly when decreasing the frequency, but also when approaching the critical point, since its proximity determines the strength of the thermomechanical coupling. Conse-

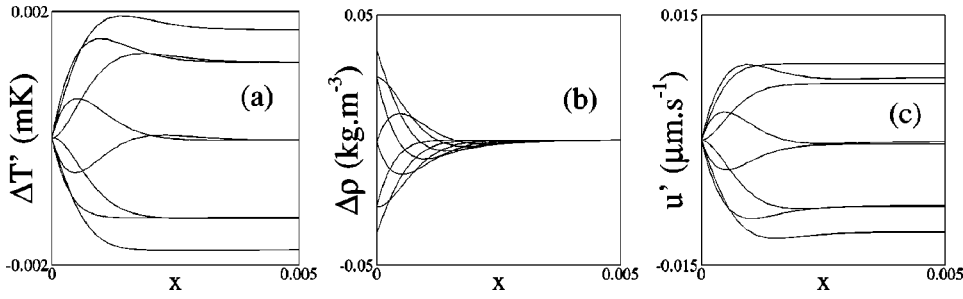


FIG. 7. Thermomechanical coupling in the boundary layer: temperature (a), density (b) and velocity (c) profiles over one period of oscillation ($f' = 5$ Hz, $\Delta T'_i = 15$ mK, $A' = 0.1$ m s $^{-2}$).

quently, the crossover between the medium and quasi-solid regimes occurs at higher frequencies if the fluid is initially closer to the critical point (not plotted; *see* Ref. 18). Typically, the quasi-solid regime could be triggered by g-jitters aboard a space station, since it appears for frequencies lower than a few tens of Hertz at 15 mK above the critical point. This should thus concern a large number of microgravity experiments on critical phenomena.

Lastly, let us add that a very good agreement has been found between our numerical results and those obtained from asymptotic methods,¹¹ as shown by the comparison reported in Table I.

IV. LOW-FREQUENCY VIBRATIONS IN A SQUARE CAVITY

A. Rescaling and modeling

On the acoustic time scale, the time needed to perform one oscillation increases as the frequency decreases. Two-dimensional computations at low frequency would then require a lot of computational time.

Therefore, time and velocity are rescaled with respect to vibration:

$$t = t' f', \quad \tilde{v} = \tilde{v}' / L' f'.$$

Additionally, since a description of acoustic waves is not necessary, an acoustic filtering procedure¹⁹ must be applied to ensure a relatively good convergence rate of our iterative algorithm (here, SIMPLER¹²). This leads to pressure splitting:

$$P = P^{(0)} + \gamma_0 \text{Ma}^2 P^{(1)},$$

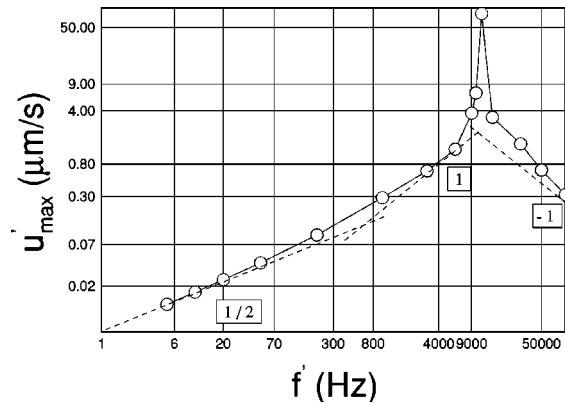


FIG. 8. The three different regimes: maximum velocity versus frequency ($\Delta T'_i = 15$ mK, $A' = 0.1$ m s $^{-2}$).

with

$$\text{Ma} = \frac{L' f'}{c_0} \ll 1,$$

a characteristic small Mach number. $P^{(0)}$ represents the homogeneous and constant part of the pressure and $P^{(1)}$ the dynamic pressure.

The momentum equation is then

$$\frac{\partial}{\partial t}(\rho \tilde{v}) + \nabla \cdot (\rho \tilde{v} \otimes \tilde{v}) = -\nabla P^{(1)} + \frac{\epsilon}{\text{Ma}} \left[\nabla^2 \tilde{v} + \frac{1}{3} \nabla (\nabla \cdot \tilde{v}) \right] + \rho A \sin(2\pi t) \tilde{e}_x, \quad (9)$$

with

$$A = A' L' / (L' f')^2.$$

The other conservation equations are written in the following form:

$$\nabla \cdot \tilde{v} = \frac{(1-b\rho) \frac{dP}{dt} - \frac{\gamma_0 \epsilon}{\text{Pr}_0 \text{Ma}} \nabla \cdot (\lambda \nabla T)}{-\gamma_0 (P + a\rho^2) + 2a\rho^2 (1-b\rho)}, \quad (10)$$

$$\begin{aligned} \frac{\partial}{\partial t}(\rho T) + \nabla \cdot (\rho T \tilde{v}) &= \frac{(\gamma_0 - 1)}{\gamma_0} (1-b\rho) \frac{dP}{dt} \\ &- 2a\rho^2 \frac{(\gamma_0 - 1)}{\gamma_0} (1-b\rho) \nabla \cdot \tilde{v} \\ &+ \frac{\epsilon}{\text{Pr}_0 \text{Ma}} \nabla \cdot [\lambda \nabla T], \end{aligned} \quad (11)$$

$$P^{(0)} + \gamma_0 \text{Ma}^2 P^{(1)} = \frac{\rho T}{1-b\rho} - a\rho^2 \left(a = \frac{9}{8}, b = \frac{1}{3} \right). \quad (12)$$

$P^{(1)}$ must be taken into account in the equation of state to allow the density variations that are needed for fluid motion when a homogeneous acceleration field is imposed in the absence of temperature inhomogeneities. The above continuity and energy equations have been reformulated by

TABLE I. A comparison between numerical and analytical results for $\Delta T'_i = 15$ mK, $A' = 0.1$ m s $^{-2}$: present calculations (1) and values obtained from the solution of the asymptotic analysis given in Ref. 11 (2).

f' (Hz)	5	10	20	50	200	1000	3000
u'_{max} ($\mu\text{m s}^{-1}$) (1)	0.0115	0.0166	0.0242	0.0404	0.094	0.29	0.652
u'_{max} ($\mu\text{m s}^{-1}$) (2)	0.0113	0.0163	0.0237	0.0397	0.092	0.28	0.668

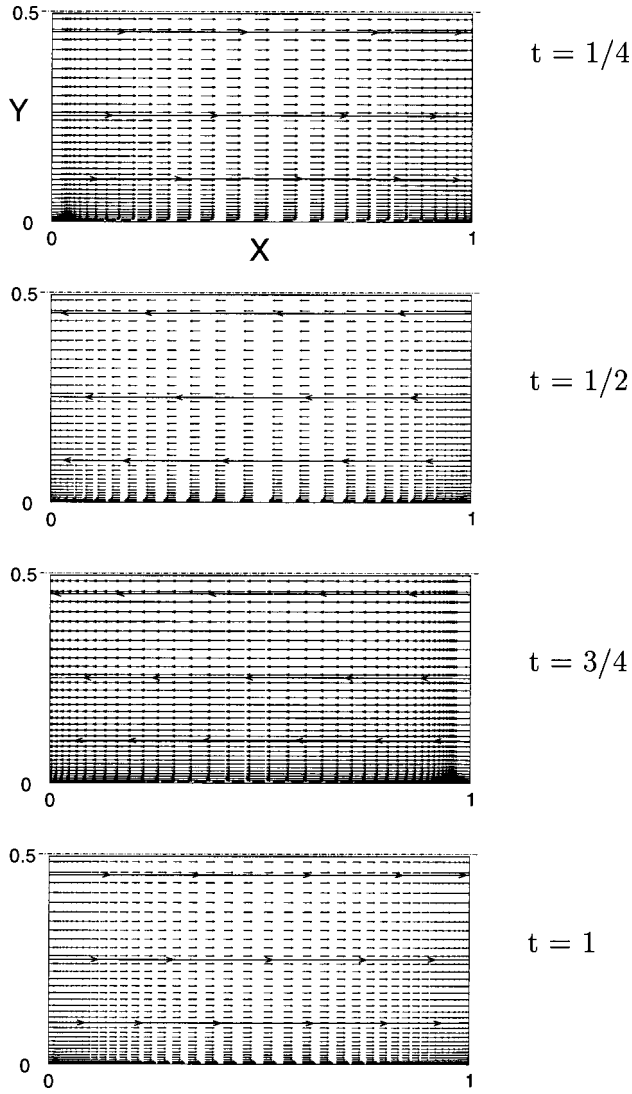


FIG. 9. Velocity field evolution in the lower half of the cell when the $y=0$ boundary is insulated ($\Delta T_i = 15$ mK, $f' = 20$ Hz, $A' = 0.1$ m s $^{-2}$).

combination so that the source term, dP/dt [in fact, $\gamma_0 Ma^2 dP^{(1)}/dt$], appears explicitly and numerically generates the correct coupling.

Let us add that, to simplify the computation, numerical calculations were only performed on the lower half of the

cavity, because of the configuration symmetry along the axis: $y=0.5$. The assumption of symmetry leads to the boundary conditions:

$$\frac{\partial T}{\partial y}(y=0.5)=0, \quad \frac{\partial u}{\partial y}(y=0.5)=0, \quad v(y=0.5)=0. \quad (13)$$

B. Adiabatic longitudinal wall

In order to isolate the role of the wall shear stresses on the fluid flow, we first consider the case in which the additional boundaries are thermally inactive:

$$\frac{\partial T}{\partial y}(y=0)=0. \quad (14)$$

The velocity field obtained on one period of oscillation is shown in Fig. 9. It appears that the fluid response remains almost one-dimensional. Figure 10 shows that the quasi-solid regime is not affected by the presence of the lower wall, except very close to it, where a boundary layer forms. The evolution of this viscous boundary layer is shown in Fig. 11 (at the center of the lower wall).

This evolution is similar to that of the Stokes boundary layer, which forms when a flat plate oscillates in an infinite fluid layer at rest.²⁰ The periodic detachment of the boundary layer provokes transversal propagating waves which strongly damp out in the bulk, as described by the Stokes solution:

$$u'(y') = u'_0 e^{-y'/\delta'} \sin(2\pi f' t' - y'/\delta'), \quad (15)$$

with

$$\delta' = \left(\frac{\nu'}{\pi f'} \right)^{1/2}. \quad (16)$$

δ' represents a length characteristic of the penetration depth (ν' is the kinetic viscosity of the fluid). Our results are in good agreement with the value deduced from this expression (with $\mu'_0 = 3.45 \cdot 10^{-5}$ kg m $^{-1}$ s $^{-1}$, $\delta'/L' \sim 3 \cdot 10^{-3}$, and $y'/\delta' \sim 2\pi$ for $y \sim 2 \cdot 10^{-2}$, about the same as the wave length that can be observed in Fig. 11). Figure 12 shows that the vibration frequency is the only parameter which determines this thickness for a given fluid, and its variations are found to satisfy the dependence predicted by relation (16). Thus, in spite of the presence of the transversal walls (x

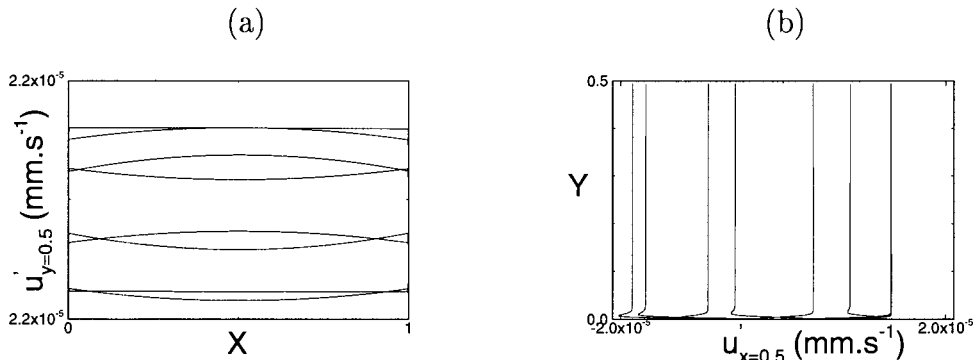


FIG. 10. Longitudinal velocity profiles along the vibrational direction (a) and in the transversal direction (b).

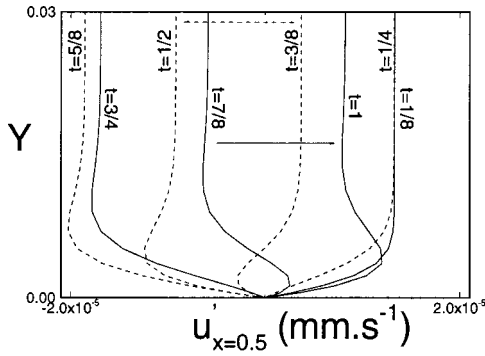


FIG. 11. Evolution of the longitudinal velocity profile in the boundary layer ($\Delta T'_i = 15$ mk, $f' = 20$ Hz, $A' = 0.1$ m s $^{-2}$).

=0 and $x=1$) and a pressure gradient, it can be said, inversely, that the results obtained for an infinite oscillating plate seem to remain valid.

Here, no singular behavior of the Stokes-like boundary layer is observed when approaching the critical point [see Figs. 11 and 12(a)], and the only specificity of this layer is that it is much thinner than that of CO $_2$ taken in normal conditions because of the small kinematic viscosity it has near-critical conditions (the critical density of CO $_2$ is $\rho'_c = 467.8$ kg \cdot m $^{-3}$). Hence, the quasi-solid regime demonstrated in one dimension can be considered to be unaffected by the presence of longitudinal boundaries when they are insulated.

C. Thermostatted wall

One very specific feature of near-critical fluids is the strong thermomechanical coupling which they obey. It is then logical to consider the case in which the longitudinal walls are thermostatted:

$$T(y=0) = 1 + \Delta T'_i. \quad (17)$$

Let us add that such conditions are more likely to be fulfilled in the experiments than adiabaticity, since it has been shown recently that, due to the piston effect and to the specific thermophysical properties of a near-critical fluid, boundary walls made of usual insulating materials cannot ensure the absence of heat losses from the fluid.^{21,22}

The velocity field evolution obtained with such thermal boundary conditions is illustrated in the lower half of the cavity in Fig. 13. The fluid oscillation therefore has more two-dimensional properties, as illustrated by the curvature of

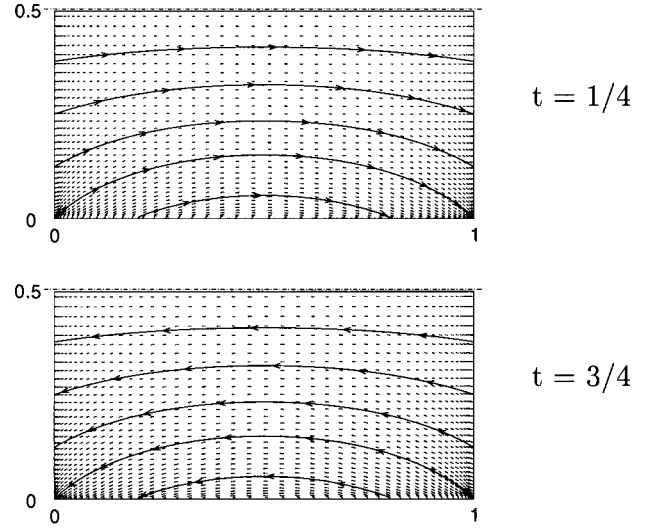


FIG. 13. Velocity field evolution in the lower half of the cell when the $y=0$ boundary is thermostatted ($f' = 20$ Hz, $\Delta T'_i = 0.1$ K, $A' = 0.1$ m s $^{-2}$).

the stream lines. This curvature is more pronounced close to the longitudinal wall, i.e., close to its origin. Since this wall is thermostatted, a thermal boundary layer forms due to the linear temperature oscillation (in the x -direction) in the bulk [Fig. 14(a)]. Thus, as in the boundary layers present along the “vertical” (y -directed) walls, thermomechanical coupling occurs which generates, by dilation or contraction of the fluid, the “vertical” motion illustrated in Fig. 14(b). This causes the curvature of the stream lines, and, because of their inhomogeneity along the longitudinal wall, the additional kinetic energy variations also make the longitudinal velocity inhomogeneous outside the dynamic boundary layer [Fig. 14(c)].

In such conditions, the one-dimensional approximation of the fluid response is far less justified, and the quasi-solid regime is affected over a wider area.

V. CONCLUSION

The numerical results presented in this paper cast some new light on the question of the behavior of a near-critical fluid confined in a thermostatted cell and submitted to low-frequency vibrations in the absence of gravity.

By first considering a one-dimensional fluid layer, we confirmed the theoretical predictions made earlier.¹¹ At low frequencies and close to the critical point, a fluid tends to

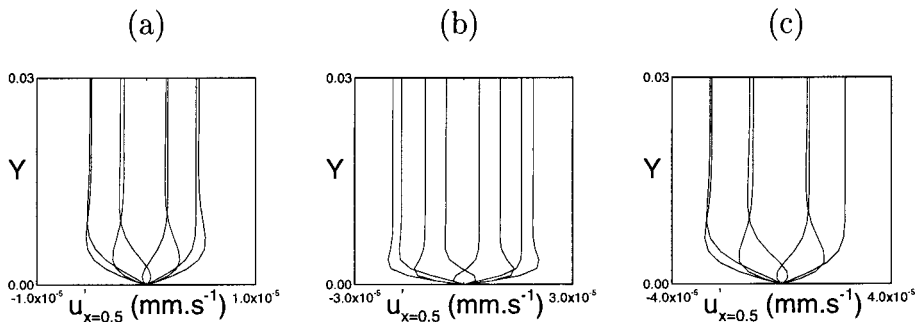


FIG. 12. Velocity profile in the boundary layer: (a) $\Delta T'_i = 0.2$ K, $f' = 20$ Hz, $A' = 0.1$ m s $^{-2}$ (b) $\Delta T'_i = 0.2$ K, $f' = 100$ Hz, $A' = 0.1$ m s $^{-2}$ (c) $\Delta T'_i = 0.2$ K, $f' = 20$ Hz, $A' = 0.5$ m s $^{-2}$.

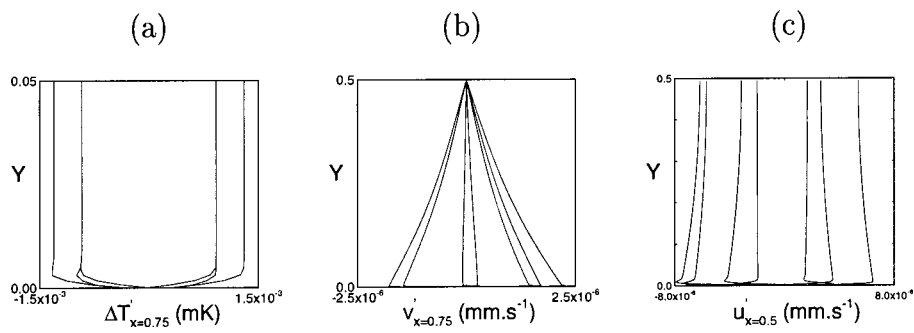


FIG. 14. Temperature (a), transversal velocity (b) and longitudinal velocity (c) when the lower wall is thermostated.

oscillate like a solid body between two highly compressible layers. On the basis of these results, a two-dimensional study was then performed, showing that the wall shear stresses, parallel to the direction of vibration, do not affect the fluid flow, since the dynamic boundary layers forming along the wall remain very thin. In a square cavity, the low-frequency regime is affected only if the longitudinal boundaries are thermostated. In such cases, longitudinal thermal boundary layers form, and strong thermomechanical coupling occurs which provokes the curvature of the stream lines.

The dynamics exhibited in the present study should be considered by those aiming to study near-critical fluids in micro-gravity, since the low-frequency regime is likely to be triggered by g-jitters and thus affect the inertia of an experimental device. They also suggest that thermovibrational convection in near-critical fluids should have some very specific properties.

¹K. Nitsche and J. Straub, "The critical 'hump' of C_v under microgravity, results from the D-Spacelab experiment 'Wärmekapazität,'" *Proceedings of the 6th European Symposium on Material Sciences Under Microgravity Conditions*, ESA SP-256, 1987.

²M. Bonetti, F. Perrot, D. Beysens, and Y. Garrabos, "Fast thermalization in supercritical fluids," *Phys. Rev. E* **49**, 4779 (1994).

³T. Fröhlich, P. Guenoun, M. Bonetti, F. Perrot, D. Beysens, Y. Garrabos, B. Le Neindre, and P. Bravais, "Adiabatic versus conductive heat transfer in off-critical SF_6 in the absence of convection," *Phys. Rev. E* **54**, 1544 (1996).

⁴Y. Garrabos, M. Bonetti, D. Beysens, F. Perrot, T. Fröhlich, P. Carlès, and B. Zappoli, "Relaxation of a supercritical fluid after a heat pulse in the absence of gravity effects: theory and experiments," *Phys. Rev. E* **57**, 1 (1998).

⁵A. Onuki and R. A. Ferrell, "Adiabatic heating effect near the gas-liquid critical point," *Physica A* **164**, 245 (1990).

⁶B. Zappoli and P. Carlès, "Thermoacoustic nature of the critical speeding-up," *Eur. J. Mech. B/Fluids* **14**, 41 (1995).

⁷B. Zappoli, S. Amiroudine, P. Carlès, and J. Ouazzani, "Thermoacoustic and buoyancy-driven transport in a square side heated cavity filled with a near critical fluid," *J. Fluid Mech.* **316**, 53 (1996).

⁸B. Zappoli, A. Jounet, S. Amiroudine, and A. Mojtabi, "Thermoacoustic heating and cooling in near-critical fluids in the presence of a thermal plume," *J. Fluid Mech.* **388**, 389 (1999).

⁹M. Gitterman, "Hydrodynamics of fluids near a critical point," *Rev. Mod. Phys.* **50**, 85 (1978).

¹⁰S. Amiroudine, P. Bontoux, Ph. Larroué, B. Gilly, and B. Zappoli, "Direct numerical simulation of unsteady instabilities inside a near-critical fluid layer under Rayleigh-Bénard configuration," submitted to *J. Fluid Mech.*

¹¹P. Carlès and B. Zappoli, "The unexpected response of near-critical fluids to low-frequency vibrations," *Phys. Fluids* **7**, 2905 (1995).

¹²S. V. Patankar, *Numerical Heat Transfer and Fluid Flow* (Hemisphere, Washington, DC, 1980).

¹³S. V. Patankar and D. P. Spalding, "A calculation procedure for heat, mass and momentum transfer in three-dimensional parabolic flows," *Int. J. Heat Mass Transf.* **15**, 1787 (1972).

¹⁴R. Peyret and T. D. Taylor, *Computational Methods for Fluid Flow* (Springer-Verlag, New York, 1983).

¹⁵S. Amiroudine, J. Ouazzani, B. Zappoli, and P. Carlès, "Numerical solutions of 1D unsteady hypercompressible flows using finite volume methods," *Eur. J. Mech. B/Fluids* **16**, 665 (1997).

¹⁶B. Zappoli, "Response of a solid-gas growth interface to a homogeneous time dependent acceleration field," *Int. J. Heat Mass Transf.* **33**, 9 (1990).

¹⁷B. Zappoli and P. Carlès, "The speeding up of heterogeneous reactions in near-critical phases," *Acta Astron.* **38**, (1) (1996).

¹⁸A. Jounet, "Numerical simulation of the piston effect in near-critical fluids in the presence of thermal or mechanical disturbance," IMFT-UPS, Ph.D. thesis, Toulouse, France, 1999.

¹⁹S. Paolucci, "On the filtering of sound from the Navier-Stokes equations," SAND 82-8257, 1982.

²⁰L. Landau and E. Lifchitz, *Mécanique des Fluides* (Ellipse, Ed. Mir, 1994).

²¹A. Jounet, B. Zappoli, and A. Mojtabi, "Numerical simulation of the Piston Effect with realistic boundary conditions," *C. R. Acad. Sci. Paris* **327**, 991 (1999).

²²A. Jounet, B. Zappoli, and A. Mojtabi, "Rapid thermal relaxation in a near-critical fluid with boundary effects taken into account," submitted to *Phys. Rev. Lett.*